RSC Advances

ROYAL SOCIETY OF CHEMISTRY

www.rsc.org/advances

The real active sites over Zn-Cr catalysts for direct synthesis of isobutanol from syngas: Structure-Activity relationship

Shaopeng Tian, [a,b] Sichen Wang, [c] Yingquan Wu, [a,b] Junwen Gao, [c] Hongjuan Xie, [a] Xiaoli Li, [a,b] Guohui Yang, [a] Yizhuo Han [a] and Yisheng Tan*[a]

([a] *State Key Laboratory of Coal Conversion, Institute of Coal Chemistry, Chinese Academy of Sciences, Taiyuan, Shanxi 030001, China*

[b] *University of the Chinese Academy of Sciences, Beijing 100039, China*

[c] *Shaanxi Yanchang Petroleum (Group) Corp. Ltd., Xi'an 710075, P. R. China)*

**Tel.: +86 351 4044287. E-mail address: tan@sxicc.ac.cn (Y. Tan)*

Abstract

A series of Zn-Cr oxides nanoparticles were prepared by a coprecipitation procedure. The structure of different catalysts was investigated by X-ray Absorption Fine Structure (XAFS), X-ray photoelectron spectroscopy (XPS), Temperature programed reduction of hydrogen (H_2-TPR) and in situ infrared spectrum (in situ IR). Both EXAFS and XANES demonstrated the cation disorder distribution became more serious with decreasing annealing temperature and increasing Zn/Cr molar ratios. The cation distribution also affected the oxygen state on the surface over Zn-Cr spinel. The population of surface hydroxyl species increased with more serious caiton disorder distribution and they facilitated the formate formation which was a significant intermediate C1 species for alcohol synthesis. This study was the first time to investigate the situation of cation distribution in Zn-Cr spinel by XAFS and related it to catalyst performance. The results revealed that the isobutanol productivity

presented a linear relationship to the level of cation disorder distribution in Zn-Cr spinel, unambiguously revealing the real active sites and structure-activity relationship.

Keywords: CO hydrogenation; isobutanol; Zn-Cr catalyst; cation distribution.

1. Introduction

With the increasing price of petroleum, environmental concerns and gasoline additive octane demands, the need for petroleum-free routes to value added chemicals will continue to intensify in the future.[1-6] The synthesis of higher alcohols from syngas (a mixture of CO and H_2) has roused considerable interest due to their potential application as good gasoline additives or alternative motor fuel for reducing the exhaust emission. [7, 8] Among the higher alcohols, isobutanol is considered as one of the most important species among coal-based clean synthetic fuels and chemical intermedium. It has been confirmed to be a better and cleaner automobile fuel with high octane number and can be used to produce plasticizer, medicine and antiager, etc. [4, 5, 9] Furthermore, isobutanol had been approved as gasoline additives by U.S. Environmental Protection Agency (EPA) in 2010. The rapid increase of isobutanol consumption requires a low cost manufacturing approach. A particularly promising non-noble metal family of catalysts, $ZnCr_2O_4$-based catalysts modified with potassium has been widely studied due to its longer time for retaining high activity, less severe coke deposition, and ability to form higher alcohols with a high selectivity to isobutanol. [10-13] The selectivity of methanol plus isobutanol is equal or greater than 94% in alcohol phase product for Zn-Cr oxides catalyst. That will simplify the process

of separation in isobutanol production and contributes greatly to the industrialization of isobutanol. Additionally, the origin of this abnormal high selectivity for isobutanol is also the motivation for understanding this catalytic process and real active sites for isobutanol in detail.

Since 1980s, Zn-Cr based oxides have been extensively studied and some pioneering work and excellent reviews have been published on this subject.[14, 15] Many studies focused on the mechanism of the reaction and the true active sites for isobutanol formation. [3, 16] However, there is still debate about the real active sites for isobutanol formation on Zn-Cr oxides catalyst. William S. Epling [11, 12] believed that the excess ZnO on Zn/Cr spinel was the active site while Zn/Cr spinel acted only as a high-surface-area support while Massimo Bertoldi [17-19] and Noritastsu [20] held the point that the non-stoichiometry phase led the catalytic activity to form alcohol. In fact, our group also made much effort to study the pathway and the real active sites of isobutanol formation from syngas. Wu [3, 4, 9] believed that the mechanism of isobutanol formation is that C_1 intermediate (formyl) addition at α-carbon on methanol to form C_{2+} alcohols and then C_{2+} alcohols underwent an aldol-condensation to form isobutanol. Kou [6, 20] held the point that the non-stoichiometry phase was the real active site for isobutanol formation on Zn-Cr spinel catalyst.

In recent years, it has been shown that $ZnCr_2O_4$ spinel can adopt normal and partially cation disorder distribution spinel structures. As a result, the physical and chemical properties can be tailored through the variation of cations on the tetrahedral and octahedral coordination sites.[21-24] On another front, X-ray absorption structure

(XAS) spectroscopy is a powerful tool to investigate the local structure of metal oxides. Both EXAFS and XANES provide valuable information.[25] Recently, they have been used to investigate the cation distribution in spinels, such as $CuFe_2O_4$, $ZnFe_2O_4$, $MnFe_2O_4$, etc. [24, 26-30] Surprisingly, merely articles deal with the structure and the situation of cation distribution in Zn-Cr spinel.

According to this, we present an X-ray absorption structure (XAS) study on the Zn and Cr distribution in $ZnCr_2O_4$ nanoparticles and focus on the relationship between the isobutanol formation and the cation distribution in Zn-Cr spinel catalyst in this manuscript. A series of Zn-Cr oxides nanocatalysts with different degrees of cation disorder distribution were obtained by a typical coprecipitation method. Catalysts were then characterized by XAFS, XPS, in situ IR and H_2-TPR to clarify the real active sites over Zn-Cr catalyst for isobutanol formation from syngas and confirm our conjecture: the structure-active relationship.

2. Experimental methods

2.1 Preparation of catalysts

Zn-Cr oxides samples were prepared by a typical coprecipitation procedure. Appropriate amounts of starting materials $Zn(NO_3)_2 \cdot 6H_2O$ mixed $Cr(NO_3)_3 \cdot 9H_2O$ and $(NH_4)_2CO_3 \cdot CH_3NO_2$ were dissolved in 800mL of deionized water, respectively. Then the two kinds of solutions were pumped together by peristaltic pumps in a well-stirred thermostated container with pH of 9 at 60 ^oC. Next, the dark green suspension was aged for 15h, then filtered, washed thoroughly by deionized water at 60 ^oC, and dried at 100 ^oC overnight. Dried samples was milled into powders and

annealed at 350 ^{o}C for 6h to remove carbonates, etc. Then, the dark powders were impregnated with 3wt% K_2O as a promotor using potassium carbonate and the incipient wetness method. Finally, the catalysts were dried at 100 ^{o}C for 12h and calcined at from 400 to 700 ^{o}C for 6h in order to form the corresponding Zn-Cr spinel-like or spinel oxides. Different ratios of Zn/Cr catalysts would be got by controlling the amounts of starting materials zinc nitrate and chromium(Ⅲ) nitrate. Catalysts could be labeled as ZC-0.5-700, ZC-0.5-550, ZC-0.5-400, ZC-0.65-400 and ZC-0.8-400, respectively. For the ZC-0.5-700, the "0.5" and "700" represented molar ratio of Zn to Cr and calcination temperature respectively, the rest of catalysts are similar.

2.2 Characterization of catalysts

2.21 XAFS Data acquisition

The Zn and Cr K-edge XAFS spectra of all samples were measured in the transmission mode at the beamline BL14W1 of the Shanghai Synchrotron Radiation Facility (SSRF). The storage ring was operated at 3.5 GeV under "top-up" mode with a constant current of 250 mA. A double crystal Si (111) monochromator was used for the experiments. The powder samples were homogeneously smeared on the Scotch adhesive tape, and several layers were folded to reach the optimum absorption thickness ($\Delta\mu d \approx 1, \Delta\mu$ is the absorption edge jump and d is the physical thickness of the sample)

2.22 XAFS Data Analysis

XAFS data were analyzed with the ATHENA and ARTEMIS code of Ravel. The energy thresholds were determined as the maxima of the first derivative. Absorption curves were normalized to 1, and the EXAFS signals χ(k) were obtained after the removal of the preedge and post-edge background. The Fourier transform (FT) spectra were obtained as $k^3\chi(k)$ with a Hanning window in the range 3 −14.5 $Å^{-1}$ for the Zn K-edge and 3 −13.5 $Å^{-1}$ for the Cr K-edge. Theoretical amplitude and phase-shift functions were calculated with the FEFF8.6 code using the structure parameters of the normal spinel structure of $ZnCr_2O_4$. Due to the transferability of amplitude and phase shifts, the coordination parameters of unknown samples can be obtained by fitting the experimental curves with theoretical amplitudes and phase shifts.

2.23 XANES Calculation

Zn K-edge XANES simulations based on self-consistent multiple-scattering (MS) theory were performed using FEFF 8.6 code with the Hedin –Lundqvist (H −L) exchange potential. A 57-atom cluster (radius 0.53 nm) was used to calculate the self-consistent field (SCF) muffin-tin atomic potential, and a 221-atom cluster (radius 0.80 nm) for full-multiple scattering (FMS) XANES calculations was considered. The normal spinel $ZnCr_2O_4$ was used as the model structure.

2.24 XPS, IR and H_2-TPR analysis

The XPS patterns were recorded using an AXIS ULTRA DLD X-ray photoelectron spectrometer, equipped with a multichannel detector. Charge referencing was done against adventitious carbon (C 1s, 284.8 eV). A Shirley-type background was subtracted from the signals. The recorded spectra were fitted using

Gauss–Lorentz curves to determine the surface composition of different samples. IR Spectra of CO adsorption and desorption were obtained with a TENSOR-27 in the range from 4000 to 1000 cm^{-1} with 4 cm^{-1} resolution. Before CO adsorption, all of catalysts were reduced with a 10% hydrogen-in-nitrogen mixture for 0.5 h at 400 ^{o}C on line. CO adsorption was taken at 400 ^{o}C and after 0.5 h of pure Ar flow at the same temperature and the adsorbates existing on the surface of different Zn-Cr spinel catalysts would be measured.

2.25 Activity measurements

Each of these catalysts was reduced with a 10% hydrogen-in-nitrogen mixture for 4 h at 400 ^{o}C on line. Then, these catalysts were tested for isobutanol catalytic activity in a fixed bed using a feed gas of 2.6:1 H_2 and CO mixture at a space velocity of 3,000 h^{-1}. The reactions were run at temperature 400 ^{o}C and pressure 10 MPa. The products were analyzed by four on-line GC during the reaction. Inorganic gas products consisted of CO, H_2, H_2O and CO_2 were detected online by thermal conductivity measurements using a GC4000A (carbon molecular sieves column). The organic gas products consisted of hydrocarbons and methanol were detected online by flame ionization measurements using a GC4000A (GDX-403 column). The alcohol products in liquid phase were detected by flame ionization measurements using a GC-7AG (Chromsorb101). The H_2O and methanol products in liquid phase were detected by thermal conductivity measurements using a GC4000A (GDX-401column).

3 Results and discussion

3.1 XANES Analysis

Normalized Zn K-edge XANES spectra of samples are shown in Fig. 1. There are three resolved peaks and a significant shoulder at the white line region, which reflects the electronic transition from zinc 1s core level to unoccupied states of p type.[31] The most striking features due to cation exchange in $ZnCr_2O_4$ at the Zn-K edge appeared around 9668 eV and 9680 eV named feature A and feature B. Feature A increases while feature B decreases in amplitude with the decreasing annealing temperature and increasing Zn/Cr molar ratios. In a similar report for the spinel structure of $ZnFe_2O_4$, Stewart et al. [31] have shown that feature A increases while feature B decreases for the Zn K-edge XANES spectrum when the degree of cation disorder distribution increases. It is highly probable that these changes have the same origin for $ZnCr_2O_4$. To support this hypothesis, S. Chen et al. [32] also performed Zn K-edge XANES simulations for the normal $ZnCr_2O_4$ structure and for isolated Zn atom substitutionally replacing Cr at octahedral sites and the calculated spectra showed a similar change as we observed here. Hence, a conclusion could be taken cautiously that the change trend of feature A and feature B shows an important local structural change in $ZnCr_2O_4$ spinel which results from considerable zinc cations transference from tetrahedral to octahedral sites. A close look of absorption-edge (see inset in Fig. 1, upper left side) revealed that it moved to higher energy, implying these samples owned higher valence and more oxide vacancies, which should also due to the more serious cation disorder distribution.

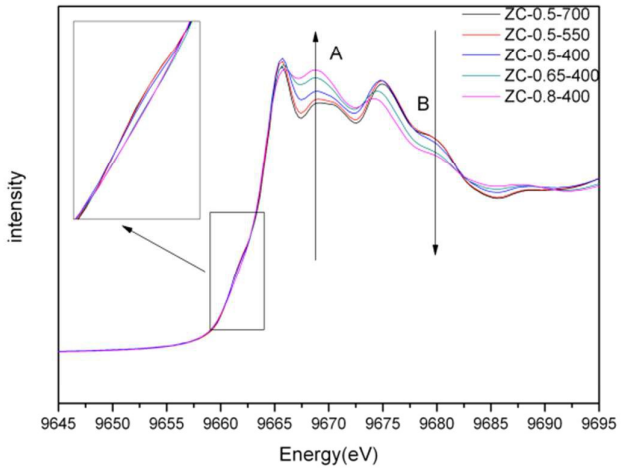

Fig.1 The normalized XANES spectra for the Zn-K-edge.

Fig. 2 showed the normalized Cr K-edge XANES spectra. The pre-edge peak (see inset in Fig. 2, upper left corner) increaseed while the absorption-edge was shifted to higher energy (see inset in Fig. 2, bottom right corner) with decreasing annealing temperature and increasing Zn/Cr molar ratios. As we know, the pre-edge peak is due to the 1s to 3d quadrupole transitions (formally electric dipole forbidden), though the intensity of the quadrupole transition is generally very low. The increase in the intensity of the pre-edge peak can be attributed to the enhancement of the orbital p-d mixing, allowed in a tetrahedral symmetry but forbidden in the octahedral one. Thus, the increase of the pre-edge peak intensity reflects the increase of the occupation number of Cr atom in tetrahedral sites (the degree of cation disorder distribution) shown as follows: ZC-0.8-400 > ZC-0.65-400 >ZC-0.5-400 > ZC-0.5-550 > ZC-0.5-700. In addition, absorption-edge (inset in Fig. 2，bottom right side) moving to higher energy also points out the increase of the degree of cation disorder distribution. All data are well consistent with the analysis results of the Zn

K-edge.

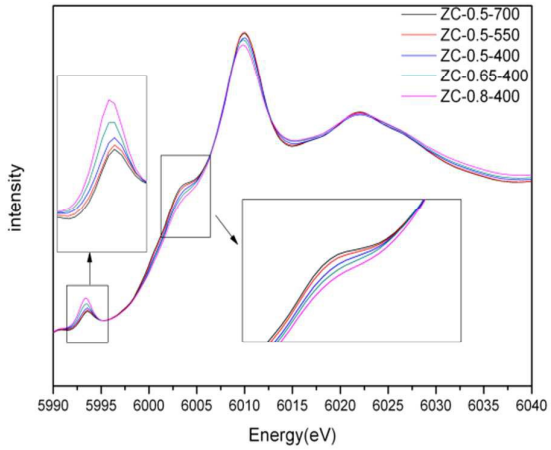

Fig.2 The normalized XANES spectra for the Cr-K-edge

3.2 EXAFS Analysis

The corresponding Fourier transforms of Zn K-edges are compared in Fig. 3. In general, in a normal structure of $ZnCr_2O_4$, the Zn atoms are tetra-coordinated by four oxygens at 1.97 Å and 12 Cr atoms are at 3.45 Å as second neighbors. On the other hand, Cr atoms are octal-coordinated by 6 O at 1.99 Å and 6 Cr atoms at 2.94 Å as second neighbors. Obviously, compared to the first coordination peak, the second coordination peak is more sensitive to the cation distribution. We may point out that, except for the two normal intensive peaks centered on around 1.6 and 3.01 Å, an additional relatively weaker peak appears at about 2.6 Å, which clearly come from the cation disorder distribution. Stewart et al.[31] have observed a similar change in the Zn K-edge of $ZnFe_2O_4$. For our samples, depending on the corresponding atomic distance mentioned above, when Zn atoms substitute to octahedral sites, a new shell would appear at about 2.94 Å (in theory) from central Zn, resulting in a new peak. In fact,

the additional peak appears at about 2.6 Å instead of at about 2.94 Å because of the instrumental error. Not surprisingly, the location of this additional peak is happening to be the second coordination distance of Cr (seen in Fig. S2). It further clearly confirmed our conclusion that some part of Zn cations would enter into the octahedral sites, signifying the cation disorder distribution appears. The new peak increased in amplitude with decreasing annealing temperature and increasing Zn/Cr molar ratios, demonstrating the trend of more serious cation disorder distribution. All analysis is consist Cr K-edge of $ZnFe_2O_4$ (seen in Fig S2).

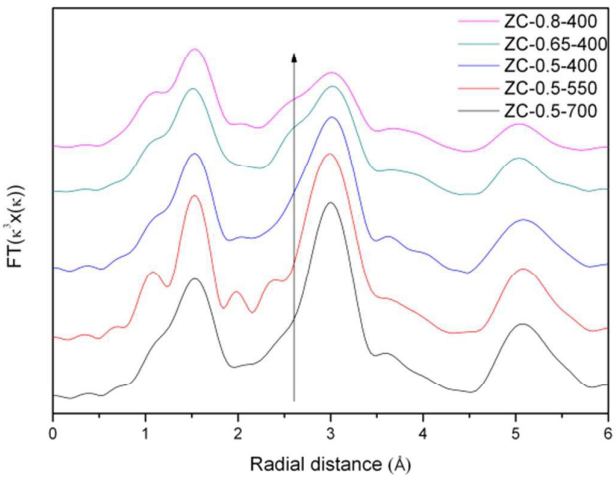

Fig. 3 The Fourier transform EXAFS signals for the Zn K-edge

In order to estimate the degree of cation disorder distribution accurately, a least-squares fitting was performed over the r-space range 0.8−3.6 Å for the Fourier transform of the Zn K-edge, following the method as described in ref 29. [33] All parameters are calculated by means of the FEFF 8.6 code. The results of fitting EXAFS data, such as lattice parameter (a), first-shell, outer-shell mean–square disorder (σ^2) and the degree of cation disorder distribution (fractional occupancy of

Zn atoms in octahedral sites), were showed in Table 1. In our computational process, all of R-facter ranged from 2.3% to 3.6% which confirmed the reliability and goodness of fitting results. As an example, the best fitting curve of the Zn K-edge for the sample ZC-0.5-700 was shown in Fig. 4 and the rests were similar.

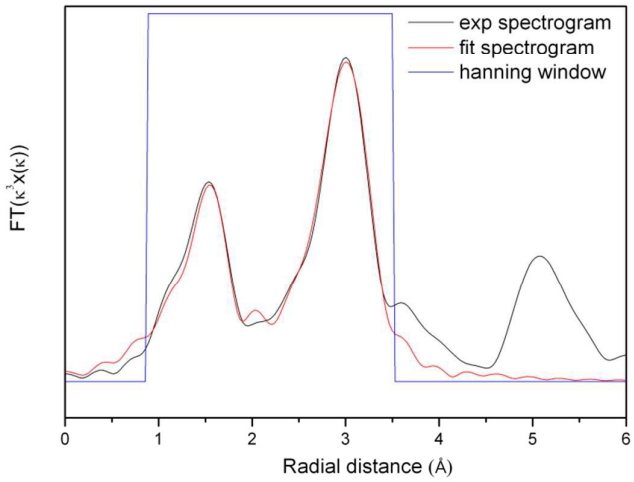

Fig. 4. Zn K-edge EXAFS spectra of ZC-0.5-700，compared with the best fit curve

The lattice parameter of ZC-0.5-700 is similar to the JCPDS standard normal spinel phase (a=b=c=8.3275). This implies that the ZC-0.5-700 sample has a normal spinel structure with rarely cation disorder distribution. However, the lattice parameter of Zn-Cr spinel phase increases continuously with decreasing calcination temperature and increasing the Zn/Cr molar ratio. In general, the lattice parameter of the spinel structure varies in accordance with the average radii of the cations in the tetrahedral and octahedral sites. That means the entire spinel framework and lattice parameter could adjust themselves by swelling or contracting to accommodate the size of the cations when the metal atoms were conversion between tetrahedral and octahedral sites [28]. Therefore, the mismatch in lattice parameter should be result

from the more serious cation disorder distribution between tetrahedral and octahedral sites. Both first-shell and outer-shell MSD (mean-square disorder) increased with decreasing the annealed temperature and increasing the Zn/Cr molar ratio, further implying the more serious cation disorder distribution.

Table. 1. Results of fitting EXAFS data to a theoretical standard. Uncertainties in the least significant digit are given in parentheses.

	Fitting results of different catalyst				
	ZC-0.5-700	ZC-0.5-550	ZC-0.5-400	ZC-0.65-400	ZC-0.8-400
lattice parameter a: (Å)	8.32(3)	8.34(2)	8.36(3)	8.44(3)	8.53(3)
First-shell MSD ($Å^2$)	0.0093(2)	0.0101(3)	0.0102(2)	0.0108(2)	0.0114(3)
Outer-shell MSD ($Å^2$)	0.0047(3)	0.0051(3)	0.0054(2)	0.0054(2)	0.0085(2)
Zn_{Bsite} (%)	0(2)	6(2)	16.5(4)	23.5(6)	27(7)
ΔE_0	-6.89(2)	-6.31(2)	-6.40(2)	-5.97(2)	-6.13(4)
R-facter (%)	2.3	2.4	2.1	3.6	3.3

'a' is the lattice parameter of Zn-Cr spinel, MSD means mean-square disorder including first-shell and outer–shell, Zn_{Bsite} is the percentage of Zn in octahedral site (the degree of cation disorder distribution), ΔE_0 is such that the energy origins lay on the rapidly rising portion of the absorption spectrum and the R-factor is a measure of the mismatch between data and fit normalized by the amplitude of the data.

Previous studies have shown that, despite the strong affinity of zinc cations for tetrahedral sites, attempts to synthesize spinel by various routes may yield significant amounts of zinc in the octahedral sites. [33] For our samples, in fact, the degree of cation disorder distribution is about 0, 6, 16.5, 23.5 and 27% for samples of ZC-0.5-700, ZC-0.5-550, ZC-0.5-400, ZC-0.65-400 and ZC-0.8-400 respectively. It clearly reveals the variation trend of cation distribution in $ZnCr_2O_4$ spinel structure. As to the sample ZC-0.5-700, all of the Zn^{2+} cations locate in tetrahedral vacancies, demonstrating that ZC-0.5-700 sample has a normal spinel structure. Conversely, approximately 27% of Zn^{2+} ions substitute to octahedral sites for the sample annealed at 400 °C and Zn/Cr molar ratio is 0.8 (ZC-0.8-400). Furthermore, the percentage of

disordered Zn^{2+} cations (in octahedral vacancies) increases from 0% to 16.5% with decreasing the annealed temperature and increases continuously from 16.5% to 27% with increasing the Zn/Cr molar ratio.

We may draw a conclusion cautiously from EXAFS and XANES analysis that the cation disorder distribution becomes more serious with decreasing annealing temperature and increasing Zn/Cr molar ratios. Specifically, higher annealing temperatures lead to significant crystallite growth and the particle size affects the cation distribution dramatically. In general, bigger particle size means most of metals are located in the bulk, so that the metals are situated in the thermodynamically most stable sites and form normal spinel structure. As to smaller particle size, a large fraction of the metals is located on the surface. Due to surface truncation, the large number of dangling bonds will affect the bonding environment of the metals and the results indicate that the lowest-energy configurations of the metals are satisfied by parts of cation disorder distribution. Camilla Nordhei [27] also held the point that the surface metal coordination would be distorted by adsorbed oxygen and water or as a consequence of hydroxide and that lead to cation disorder distribution. This hypothesis could also be further confirmed by XPS, H_2-TPR and in situ DRIFT analysis below. In the case of Zn^{2+}-rich samples, the extra small-sized Zn cations will enter the spinel lattice to generate the non-stoichiometric spinel. Because of the great difference of the crystal lattice energy of ZnO and Cr_2O_3 (being 4107.25 kJ/mol and 15186 kJ/mol, respectively which mean cations located at octahedral sites are more stable than tetrahedral sites), the extra small-sized Zn cations prefer into the

octahedral sites to exacerbate further the level of disordered distribution. Z. V. Marinkovic [34] also held the same point.

In a word, annealing temperatures affects cation distribution by tailoring particle size and in the case of Zn^{2+}-rich samples the extra small-sized Zn cations will enter the spinel lattice to exacerbate further the level of cation disordered distribution. As we all know, the spinel with more serious disorder distribution have better catalytic activity since it owns more defects and oxygen vacancies which should activates the reactants easier. The physical and chemical properties also could be tailored through the variation of cations on the tetrahedral and octahedral sites and then effect dramatically on isobutanol formation.

O-XPS analysis of catalysts

O 1s XPS spectra of catalysts were shown in Fig. 5. Three oxygen signals located at 529.4, 531.1, and 532.7 eV attributed to lattice oxygen O_{latt}, surface absorbed oxygen O_{ads} and hydroxyl species O_{OH-} on the surface, respectively.[35] The molar ratio of $O_{ads}/(O_{latt} + O_{OH-} + O_{ads})$ and $O_{OH-}/(O_{latt} + O_{OH-} + O_{ads})$was obtained thanks to quantitative calculation of the corresponding peaks areas and the result was shown in Table S1. It revealed that the ratio of $(O_{OH-} + O_{ads}) /(O_{latt} + O_{OH-} + O_{ads})$ became higher following the more serious cation disorder distribution. This result could be further confirmed by the H_2-TPR study (seen in Fig. 6). As we discussed above, the spinel with cation disorder distribution is not situated in the thermodynamically most stable sites and the "metastable state" could exist steadily is due to the large number of dangling bonds (surface absorbed oxygen O_{ads} and

hydroxyl species O_{OH-}). The population of these dangling bonds increases with decreasing annealing temperature and increasing Zn/Cr molar ratios, indicating the trend of more serious cation disorder distribution.

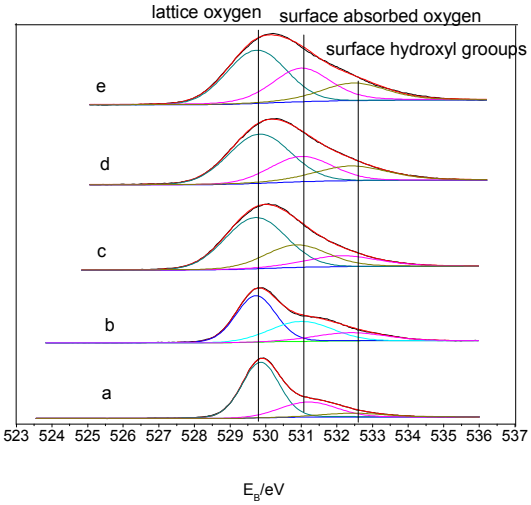

Fig.5. O 1s XPS spectra of catalysts, a: ZC-0.5-700, b: ZC-0.5-550, c: ZC-0.5-400, d: ZC-0.65-400 and e: ZC-0.8-400

H_2-TPR analysis of catalysts

Redox properties of different catalysts were evaluated by H_2-TPR and the results were displayed in Fig. 6. For each catalyst, just one main hydrogen consumption peak was observed in the temperature range of 300–400 ^oC and the area was becoming larger with more serious cation disorder distribution. It was reported that Zn^{2+} and Cr^{3+} were very difficult to be reduced in the Zn-Cr spinel. However, our catalysts are situated in the "metastable state" due to the cation disorder distribution and that makes our catalysts could be reduced much easier. Besides, In Fig.1 and Fig. 2, the absorption-edge of both Zn and Cr move to higher energy which means the valence of them become higher than normal spinel. The higher valence should make them could be reduced much easier.

In a word, because of the more serious cation disorder distribution, the valence of both Zn and Cr become higher and that "metastable state" needs more dangling bonds to stay steadily. It makes our catalysts could be reduced much easier and the larger hydrogen consumption should be attributed to the increase of oxygen-containing species on the surface. For our catalysts, considering the in-situ DRIFT analysis (seen in Fig. 7-1 and 7-2) and catalytic performance (seen in Table. 2), it seems that the surface hydroxyl species is not just stabilize the "metastable state" but also facilitate the alcohol synthesis.

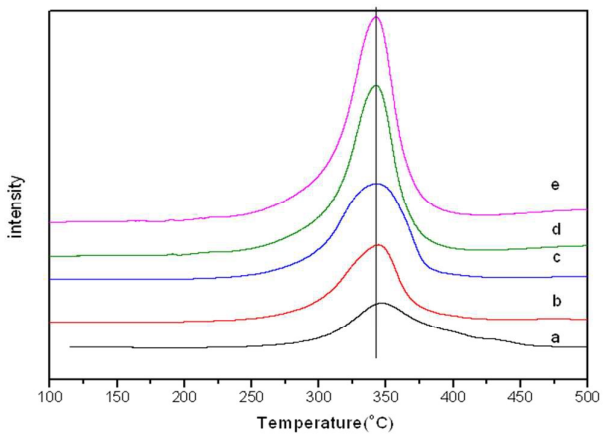

Fig. 6. H_2-TPR profiles of catalysts, a: ZC-0.5-700, b: ZC-0.5-550, c: ZC-0.5-400, d: ZC-0.65-400 and e: ZC-0.8-400

In situ DRIFTS analysis of catalysts

Additional information about the identity and population of the species was provided by an in situ DRIFTS study after adsorbing sufficient CO molecule at the reaction temperature. Fig. 7-1 showed the consumption of hydroxyl species (3400 cm^{-1}) after reacting with adsorbed CO molecule of different catalysts. The amount of hydroxyl consumption become larger with more serious cation disorder distribution, demonstrating that these catalysts owned more hydroxyl on the catalyst surface and

that was in agreement with the XPS and H_2-TPR analysis.

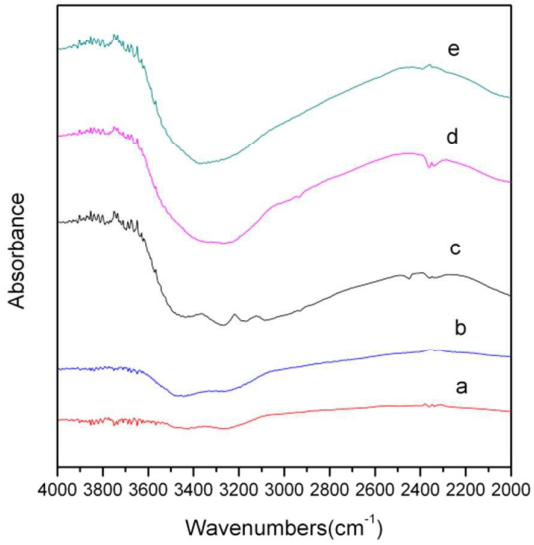

Fig. 7-1. DRIFTS spectra of CO adsorbed on catalysts upon desorption at 400 ^{o}C, a: ZC-0.5-700, b: ZC-0.5-550, c: ZC-0.5-400, d: ZC-0.65-400 and e: ZC-0.8-400

Fig. 7-2 showed the corresponding C_1 species after adsorbed CO reaction with surface hydroxyl species. Two mainly C_1 species were observed, namely: formate species [solid line: 1600 cm^{-1}, $\upsilon_{as}(CO_2^-)$; 1375 cm^{-1}, $\sigma(CH)$] and carbonates species (dot line: 1560 cm-^{1}, 1330 cm^{-1}). For catalyst ZC-0.5-700, the spectrum showed mostly adsorbed carbonates with a small formate signal. The population of the formate species increased with more serious cation disorder distribution and got maximised for ZC-0.8-400 catalyst. As to the carbonate species, however, the changing trend showed in an opposite direction.

Alexis T. Bell and co-workers [36] believed that the formation of formate species was an activated process, very likely involving the transfer of a proton from a surface hydroxyl group to adsorbed CO and the formation of carbonate species is attributed to the interactions of CO with both O^{2-} and OH^- sites on the surface of ZrO_2. By the use

of temperature programmed surface reaction (TPSR), Wachs and Madix [37] discovered that the stable intermediate on the reaction from CO/CO_2 to CH_3OH was a formate while the carbonate species could be easily converted to CO_2 which is useless for alcohol formation. K. C. Waugh [37] drew an important conclusion that formate species was a true intermediate and it was the most stable and long-lived intermediate in methanol synthesis. From discuss above, some conclusions could be drawn cautiously that formate species was a very significant intermediate for methanol synthesis and formate formation involved hydroxyl group and adsorbed CO on catalyst surface.

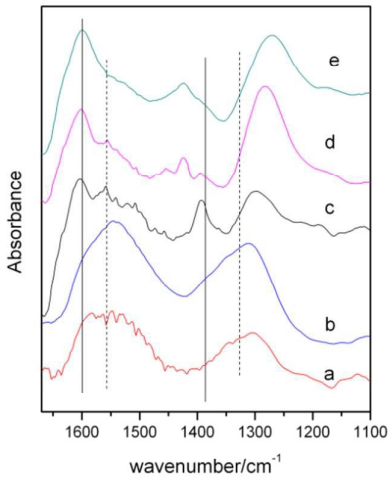

Fig. 7-2. DRIFTS spectra of CO adsorbed on catalysts upon desorption at 400 °C, a: ZC-0.5-700, b: ZC-0.5-550, c: ZC-0.5-400, d: ZC-0.65-400 and e: ZC-0.8-400

Catalysts active measurement

The information of typical catalytic performance including reaction condition was shown in Table 2. The conversion of CO using ZC-0.5-700 catalyst is extremely small, only ~10% CO being conversed, and the selectivity of isobutanol was tiny (4.44%). After lowering calcination temperature，the conversion was enhanced, ~15% and ~30% conversion of CO was obtained by ZC-0.5-550 and ZC-0.5-400 samples

and the selectivity of isobutanol was promoted from 4.44% to 10.78%. Compared the samples with different Zn/Cr molar ratios calcined at 400 ^{o}C, the conversion of CO kept ~30%, while the selectivity of isobutanol monotonously increased from 10.78% to 15.99% with increasing the Zn/Cr molar ratios.

The catalysts annealed at lower temperature showed much higher activity and much better selectivity of isobutanol. When lowing the annealing temperature from 700 ^{o}C to 400 ^{o}C, about 3 times CO conversion (from 10.04% to 30.72%) and 2 times isobutanol selectivity (from 4.44% to 10.78%) were observed. As to the catalysts with different Zn/Cr molar ratios, the catalysts present similar CO conversion (~30%) and much better isobutanol selectivity (from 10.78% to 15.99%). The outstanding capability of the catalysts should be attributed to the more serious cation disorder distribution. It is worth noting that the selectivity of methanol plus isobutanol is closely 95% in alcohol pahse which is a typical character of Zn-Cr catalysts. This should simplify the process of products separation and then contribute greatly to the industrialization of isobutanol.

The present Zn-Cr catalysts presented a lower selectivity to isobutanol than that of the Zn-Cr samples reported by William S. Epling and co-workers, [11, 12] possibly due to the differences in the reaction conditions and/or sample composition and texture. It must be stressed that the point of our present study is not to improve on the highest reported selectivity to isobutanol, but to study the active sites of isobutanol over Zn-Cr spinel catalysts.

Table. 2. Typical catalytic performance of Zn-Cr based catalysts

catalysts	CO conversion (%)	Total alcohol rate (g/ml h)	Alcohol distribution /wt%				
			Methanol	Ethanol	Propanol	Isobutanol	C_{5+} alcohol
ZC-0.5-700	10.04	0.019	87.92	3.05	3.78	4.44	0.63
ZC-0.5-550	15.81	0.034	85.23	3.26	1.49	8.34	0.58
ZC-0.5-400	30.72	0.067	83.63	1.75	1.06	10.78	0.31
ZC-0.65-400	30.43	0.075	81.45	1.68	2.16	13.19	0.51
ZC-0.8-400	30.68	0.084	79.77	1.09	2.43	15.99	0.70

Reaction conditions: Temperature=400 ^{o}C, Pressure=10 Mpa, GHSV=3000 h^{-1}

Because catalysis is a surface phenomenon, to better understand the structure-activity relationship, we set the unit of isobutanol productivity as "mg of isobutanol per m^2 of catalyst surface area per hour" instead of "mg of isobutanol per ml of catalyst per hour". The texture parameters of catalysts used here can be seen in Table. S2. Another fact what we should notice here is that the cation disorder distribution in our samples mainly involve the surface atoms because these atoms could exist in the disorder state due to large number of dangling bonds while the bulk atoms in spinel are situated in the thermodynamically most stable sites: normal spinel structure. Fig. 8 showed that the isobutanol productivity was approximately linear to the level of cation disorder distribution, confirming that the cation distribution effected dramatically on the isobutanol formation. This is the first time revealing that the productivity of isobutanol is strongly related to the cation distribution in Zn-Cr spinel investigated by XAFS. To be specific, with decrease annealing temperature and increase Zn/Cr molar ratio of Zn-Cr catalysts, the level of cation disorder distribution becomes higher. It leads less perfect crystal, more oxygen

vacancies and more defects which should lower the activation energy for isobutanol. Furthermore, the defects and vacancies affect drastically the oxygen state on catalyst surface which plays a significant role in the process of isobutanol formation.

What we must say is the conclusion of structure-activity relationship in this article is just suitable for a certain limited range. To be specific, higher annealed temperatures than 700 ^{o}C would have little influence on the structure of Zn-Cr spinel. On the other hand, it will be meaningless to prepare our catalysts at lower temperature than our reaction condition (400 ^{o}C). In the case of Zn/Cr different ratios samples, if the Zn/Cr ratio is less than 0.5，the redundant Cr cations will form Cr_2O_3 to disturb our research and if the Zn/Cr ratio is more than 0.8, some of parts of Zn cations wouldn't enter the spinel lattice but formed wurtzite crystal structure which will disturb our experience.

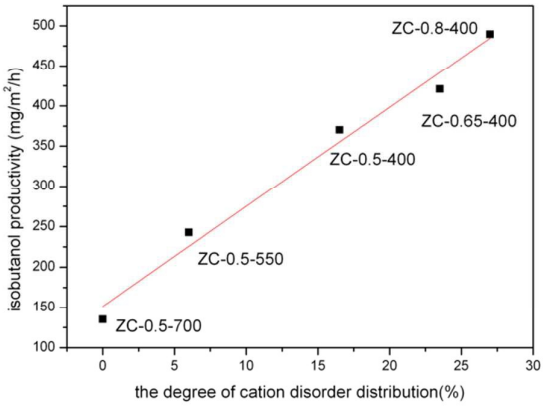

Fig. 8 The curve of isobutanol productivity with the level of cation disorder distribution

Conclusion

A series of Zn-Cr oxides nanoparticles with different degrees of cation disorder distribution were obtained by a coprecipitation and postcalcined method. Both

EXAFS and XANES were used to investigate the change of cation disorder distribution. Zn-Cr nanoparticles with a disorder distribution parameter of 27% were obtained when annealing temperature was 400 ^{o}C and the Zn/Cr ratio was 0.8. The detailed analysis demonstrates that the disorder distribution strongly depends on the annealing temperature and the Zn/Cr molar ratio. It becomes more serious with decreasing calcination temperature and increasing the Zn/Cr molar ratio.

The cation distribution will tailor the oxygen state on the surface of catalysts and affect dramatically isobutanol formation. The population of absorption-oxygen species increases with more serious caiton disorder distribution in Zn-Cr spinel. In addition, it seems that the surface hydroxyl species is not just stabilize the "metastable state" but also facilitate the formate formation species which is a very significant intermediate C_1 species for alcohol synthesis.

The isobutanol productivity is closely related to the cation disorder distribution. This clearly demonstrates that the disorder cation especially Zn cations in octahedral vacancy should be the active sites for isobutanol formation. In heterogeneous catalysis, a catalyst having a finely designed structure usually exhibits better catalytic performance. As to our research specifically, more disorder cation distribution leads more defects which effects drastically on catalysts characters and makes isobutanol formation more effectively. A better understanding of real active sites over Zn-Cr based catalysts for isobutanol formation from syngas should play a significant role to enhance the catalyst performance or design a more effective new catalyst for higher alcohol synthesis.

Acknowledgements

The authors thank the Shanghai Synchrotron Radiation Facility for providing the beamline BL14W1 for the beam time measurement. This work was supported by the National Natural Science Foundation of China (21573269), The Prospective Project of Institute of Coal Chemistry, The Chinese Academy of Sciences (No. 2011SQZBJ13) and the Cooperative Project of Shaanxi Yanchang Petroleum (Group) Corp. Ltd., China (JT1014SKF0003).

Reference

1. Y. Lu, B. Cao, F. Yu, J. Liu, Z. Bao and J. Gao, *ChemCatChem* 2014, 6, 473-478.
2. J. M. Beiramar, A. Griboval-Constant and A. Y. Khodakov, *ChemCatChem* 2014, 6, 1788-1793.
3. W. Ying-Quan, W. Si-Chen, X. Hong-Juan, G. Jun-Wen, T. Shao-Peng, H. Yi-Zhuo and T. Yi-Sheng, *Acta Phys. -Chim. Sin*, 2015, 31(1), 166-172.
4. Y. Q. Wu, H. J. Xie, Y. L. Kou, N. Tsubaki, Y. Z. Han and Y. S. Tan, *Korean J. Chem. Eng.* , 2015, 32, 406-412.
5. S. Tian, S. Wang, Y. Wu, J. Gao, Y. Bai, P. Wang, H. Xie, Y. Han and Y. Tan, *J. Mol. Catal. A: Chem.* , 2015, 404–405, 139-147.
6. Y. Kou, H. Xie, G. Liu, Y. Wu, X. Zhang, Y. Han, T. Noritatsu and Y. Tan, *J. Fuel Chem. and Tech.*, 2013, 41, 703-709.
7. G. Liu, T. Niu, D. Pan, F. Liu and Y. Liu, *Appl. Catal., A -gen* , 2014, 483, 10-18.
8. J. H. Lee, K. H. Reddy, J. S. Jung, E.-H. Yang and D. J. Moon, *Appl. Catal., A-gen* , 2014, 480, 128-133.
9. Y. Wu, H. Xie, S. Tian, N. Tsubaki, Y. Han and Y. Tan, *J. Mol. Catal. A: Chem.* , 2015, 396, 254-260.
10. L. Lietti, E. Tronconi and P. Forzatti, *J. Catal.* , 1992, 135, 400-419.
11. William S. Epling, Gar B. Hoflund, Walter M. Hart and y. D. M. Minahan, *J. Catal.*, 1997, 169, 438-446.
12. William S. Epling, Gar B. Hoflund, W. M.Hart and y. D. M. Minahan, *J. Catal.*, 1997, 172, 13-23.
13. R. G. Herman, *Catal. Today* 2000, 55, 233-245.
14. W. Keim and W. Falter, *Catal. Lett.* , 1989, 3, 59-63.
15. G. D. Piero, F. Trifiro and A. Vaccari, *J. Chem. Soc, Chem. Comm.*, 1984, 656-658.
16. J. G. Nunan, C. E. Bogdan, K. Klier, K. J. Smith, C.-W. Young and R. G. Herman, *J. Catal.* , 1989, 116, 195-221.
17. M. Bertoldi, B. Fubini, E. Giamello, G. Busca, F. Trifirò and A. Vaccari, *J. Chem. Soc., Fara. Trans.*, 1988, 84, 1405.

18. B. F. T. Gastone Del Piero, Angelo Vaccari, *J. Chem. Soc, Chem. Comm.*, 1984, 656-658.
19. E. Giamello, B. Fubini, M. Bertoldi, G. Busca and A. Vaccari, *J. Chem. Soc., Fara. Trans.,* 1989, 85, 237.
20. L. Tan, G. Yang, Y. Yoneyama, Y. Kou, Y. Tan, T. Vitidsant and N. Tsubaki, *Appl. Catal., A-gen*, 2015, 505, 141-149.
21. D. S. Nikam, S. V. Jadhav, V. M. Khot, R. A. Bohara, C. K. Hong, S. S. Mali and S. H. Pawar, *RSC Advances*, 2015, 5, 2338-2345.
22. A. Kitada, A. M. Arevalo-Lopez and J. P. Attfield, *Chem. Commun.* , 2015.
23. W. H. Kan, A. Huq and A. Manthiram, *Chem. Commun.* , 2015, 51, 10447-10450.
24. C. Reitz, C. Suchomski, J. Haetge, T. Leichtweiss, Z. Jaglicic, I. Djerdj and T. Brezesinski, *Chem. Commun.* , 2012, 48, 4471-4473.
25. W.-W. Wang, P.-P. Du, S.-H. Zou, H.-Y. He, R.-X. Wang, Z. Jin, S. Shi, Y.-Y. Huang, R. Si and Q.-S. Song, *ACS Catalysis*, 2015, 5, 2088-2099.
26. M. H. Nilsen, C. Nordhei, A. L. Ramstad, D. G. Nicholson, M. Poliakoff and A. Cabañas, *The J. Phys. Chem. C.*, 2007, 111, 6252-6262.
27. C. Nordhei, A. L. Ramstad and D. G. Nicholson, *PCCP* 2008, 10, 1053-1066.
28. M. J. Akhtar, M. Nadeem, S. Javaid and M. Atif, *J. Phys-Cond Matt.*, 2009, 21, 9.
29. D. Makovec, A. Kodre, I. Arcon and M. Drofenik, *J. Nanopart. Res.* , 2011, 13, 1781-1790.
30. D. Carta, C. Marras, D. Loche, G. Mountjoy, S. I. Ahmed and A. Corrias, *J. Chem. Phys.* , 2013, 138, 9.
31. S. Stewart, S. Figueroa, J. R. López, S. Marchetti, J. Bengoa, R. Prado and F. Requejo, *Phys. Rev. B.*, 2007, 75, 073408.
32. S. Chen, Y. Wu, P. Cui, W. Chu, X. Chen and Z. Wu, *J. Phys. Chem. C.*, 2013, 117, 25019-25025.
33. S. Calvin, E. E. Carpenter, V. G. Harris and S. A. Morrison, *Appl. Phys. Lett.* , 2002, 81, 3828-3830.
34. Z. V. Marinković, L. Mančić, P. Vulić and O. Milošević, *J. Eur. Ceram. Soc.* , 2005, 25, 2081-2084.
35. C. H. Zhang, C. Wang, W. C. Zhan, Y. L. Guo, Y. Guo, G. Z. Lu, A. Baylet and A. Giroir-Fendler, *Appl. Catal. B-Environ.*, 2013, 129, 509-516.
36. K. Pokrovski, K. T. Jung and A. T. Bell, *Langmuir*, 2001, 17, 4297-4303.
37. K. C. Waugh, *Catal. Lett.* , 2012, 142, 1153-1166.